SIAM J. SCI. COMPUT.
Vol. 31, No. 5, pp. 3301–3323


# A GENERAL PERFECTLY MATCHED LAYER MODEL FOR HYPERBOLIC-PARABOLIC SYSTEMS*

DANIEL APPELÖ† AND THOMAS HAGSTROM‡

**Abstract.** This paper describes a very general absorbing layer model for hyperbolic-parabolic systems of partial differential equations. For linear systems with constant coefficients it is shown that the model possesses the perfect matching property, i.e., it is a perfectly matched layer (PML). The model is applied to two linear systems: a linear wave equation with a viscous damping term and the linearized Navier–Stokes equations. The resulting perfectly matched layer for the viscous wave equation is proved to be stable. The paper also presents how the model can be used to construct an absorbing layer for the full compressible Navier–Stokes equations. For all three applications, numerical experiments are presented. Especially for the linear problems, the results are very promising. In one experiment, where the performance of a "hyperbolic PML" and the new hyperbolic-parabolic PML is compared for a hyperbolic-parabolic system, an improvement of *six orders of magnitude* is observed. For the compressible Navier–Stokes equations results obtained with the presented layer are competitive with existing methods.

**Key words.** perfectly matched layers, hyperbolic-parabolic systems

**AMS subject classifications.** 35L45, 35B35

**DOI.** 10.1137/080713951

## 1. Introduction.

In engineering applications it is common to encounter problems posed on large or unbounded domains, where some particular quantity is desired on a more localized domain. An example is the measurements of heat deposition inside the human brain due to electromagnetic radiation from a cell phone. There the localized domain is the brain, and the large domain is the cafe; the person being on the phone is sitting in. Another example is the design of airplanes, where it is important to minimize the engine noise transmitted into the cockpit and cabin. The localized domain is then the plane and its immediate surrounding, and the unbounded domain is the free space, extending all the way down to the ground.

Since the localized problems can be arbitrarily complex (and thus very costly to solve numerically), it is important not to waste any computational resources in domains where the simulated physical quantities are of no interest. Therefore, unbounded domains are truncated by replacing the exterior to the domain, where the simulated quantities *are* of interest, by some boundary procedure.

For problems governed by systems of hyperbolic partial differential equations, the research for such boundary procedures have a long and successful history (see, for example, the reviews [30, 13, 14, 20]). The publishing of the seminal paper by Engquist and Majda [11] in 1977 provided the mathematical foundation for the development of nonreflecting boundary conditions for hyperbolic problems and led to a very active

*Received by the editors January 22, 2008; accepted for publication (in revised form) May 8, 2009; published electronically August 5, 2009.
http://www.siam.org/journals/sisc/31-5/71395.html

†Center for Applied Scientific Computing, Lawrence Livermore National Lab, Livermore, CA 94551. Current address: Computational and Applied Mathematics, California Institute of Technology, Pasadena, CA 91125 (appelo@caltech.edu). This work performed under the auspices of the U.S. Department of Energy by Lawrence Livermore National Laboratory under Contract DE-AC52-07NA27344.

‡Department of Mathematics, Southern Methodist University, Dallas, TX 75275-0156 (thagstrom@smu.edu). The work of this author partially supported by NSF grant DMS-06010067 and ARO grant DAAD19-03-1-0146.

period of research in the field. Although many of the methods developed in the wake of [11] could, in theory, be made both local and arbitrarily accurate by increasing the order of the approximation of certain pseudodifferential operators, practitioners soon found out that it was hard to discretize the higher order approximations in a stable manner. As computers became more powerful and the numerical methods for the interior problem became better, there was a mounting need for an accurate truncation method which was also easy to implement. The invention of the perfectly matched layer (PML) by Bérenger [7] in 1994 provided such a method. Bérenger's method was instantly utilized by engineers throughout the computational electromagnetics community, and although there were some minor flaws in Bérenger's formulation [1, 2, 3], the concept of a PML proved very useful and was rapidly extended to other hyperbolic systems [22, 9, 31]. Somewhat later (motivated by blow up in some early PML models) it was understood that to construct a stable PML, equation-dependent modifications to Bérenger's original idea had to be introduced. By now, those modifications are known for many applications, but the question whether or not it is possible to construct a stable PML for all linear hyperbolic systems remains open; see [6, 4, 5].

Compared to the extensive research on domain truncation techniques for hyperbolic systems, there are very few results (that the authors know of) in the numerical analysis literature on domain truncation for *mixed hyperbolic-parabolic systems*. This may be explained, in part, by the fact that most of the mixed problems arise in the context of nonlinear problems (the most prominent example is of course the Navier–Stokes equations). For such nonlinear problems the interior methods cannot yet produce as accurate results as for simpler linear problems; thus the need for highly accurate boundary procedures has been limited. This will naturally change as the interior methods become more and more accurate.

There are, however, some contributions on domain truncation techniques for mixed hyperbolic-parabolic systems that we would like to mention. The extension of Engquist and Majda's nonreflecting boundary conditions to linear mixed systems can be found in the paper [21] by Halpern. The main difference compared to the hyperbolic problem is the additional analysis of potential boundary layers generated by the extra boundary conditions. Another approach, based on the asymptotic analysis of dissipative waves, is described in [12]. More recently, local high order nonreflecting boundary conditions based on formulations using auxiliary variables have also been investigated [18, 19].

Ad hoc damping layers (often referred to as sponge layers) have been around for a long time; see, e.g., [25, 8]. They have been used with reasonable success in nonlinear fluid dynamics computations. In particular, the more recent "super-grid-scale method" by Colonius and Ran [10] has been shown to work very well for nonlinear problems; see [15]. It is, however, known that for linear hyperbolic problems, the ad hoc layers cannot compete with PML [15]. The extension of the PML method to linear mixed hyperbolic-parabolic systems is therefore very natural. A way to extend it to such systems has already been reported, along with experimental results, in [18, 19, 17]. This is the approach we advocate, develop, and formalize here. Another possible extension is found in [24].

In this paper we study the application of the PML method to both linear and nonlinear mixed hyperbolic-parabolic systems. In section 2 we formalize the ideas outlined in [18, 19, 17] into a general PML model for mixed hyperbolic-parabolic systems of partial differential equations. The model, which can be seen as an extension of our general model for hyperbolic systems developed in [5], is also shown to possess the perfect matching property.

In section 3 we present three applications of our general model. We first consider an advection-diffusion equation and use the Sturm sequence methods developed in [16] to establish stability. We compare the efficiency of the suggested PML model to the corresponding PML model for the hyperbolic system obtained by neglecting the parabolic terms.

The second application is the linearized Navier–Stokes equations. By numerical experiments, we study how the efficiency of the PML models depends on various parameters controlling the damping properties of the layer. The results obtained are similar to those obtained for hyperbolic equations. For example, if the evanescent waves are not handled correctly, we observe the typical deterioration in performance at late times. The results for both linear problems are very encouraging; for some of the examples we observe six orders of magnitude improvement compared with results obtained by direct application of the corresponding hyperbolic PML models.

Our third and final application is the full compressible Navier–Stokes equations. For this nonlinear problem the perfect matching is lost, and the layer becomes an absorbing layer. In our numerical examples we see that, due to the loss of matching, the results are not as good as for the linear applications. However, our experiments indicate that the new layer performs reasonably well relative to Colonius' super grid method, which is designed for nonlinear problems.

Finally, in section 5 we summarize.

**2. A PML model for the hyperbolic-parabolic system.** In this paper we consider the construction of a PML model for the hyperbolic-parabolic problem

$$u_t = A_{11}u_x + A_{12}v_x + B_{11}u_y + B_{12}v_y + C_1u_{xx} + C_2u_{xy} + C_3u_{yy}, \tag{2.1}$$

$$v_t = A_{22}v_x + A_{12}^T u_x + B_{22}v_y + B_{12}^T u_y. \tag{2.2}$$

Here $u = u(x, y, t)$ and $v(x, y, t)$ are real-valued vector functions of dimension $p$ and $q$. We make the following assumptions:

(A1) All matrices $A_{ij}$, $B_{ij}$, $C_j$ are real and symmetric.

(A2) $A_{22}$ is nonsingular.

(A3) $u_t = C_1u_{xx} + C_2u_{xy} + C_3u_{yy}$ is Petrowskii parabolic, i.e.,

$$x^*(\xi_1^2C_1 + \xi_1\xi_2C_2 + \xi_2^2C_3)x > 0,\ \forall \xi_1, \xi_2 \in \mathbb{R},\ x \in \mathbb{C}^p,\ x, \xi \neq 0.$$

We consider the particular case when the problem is posed on $-\infty \leq x, y \leq \infty$, but we are only interested in the solution in $x < 0$. Assuming that the initial data are supported only on the strip $-H \leq x \leq -h$, $h > 0$ in the left halfspace, we truncate the problem by replacing the governing equations with a PML model in $x > 0$.

If $C_j = 0$, $j = 1, \ldots, 3$, the system (2.1)–(2.2) is reduced to a symmetric hyperbolic system. Such systems were discussed in [5] where we presented a very general PML model. The starting point for that construction was the eigenvalue problem

$$\begin{bmatrix} sI - ikB_{11} & -ikB_{12} \\ -ikB_{12}^T & sI - ikB_{22} \end{bmatrix} \hat{\Phi}(s, ik) = \lambda \begin{bmatrix} A_{11} & A_{12} \\ A_{12}^T & A_{22} \end{bmatrix} \hat{\Phi}(s, ik). \tag{2.3}$$

Equation (2.3) is obtained by taking the Laplace transform in time and the Fourier transform in the tangential $y$ direction, with the modal ansatz

$$[\hat{u}(s, ik, x), \hat{v}(s, ik, x)]^T = \exp(\lambda x)\hat{\Phi}(s, ik).$$

The two key properties of any PML model are the perfect matching and the exponential decay of the solution inside the layer. The latter can be accomplished by modifying the eigenvalues of (2.3), and the former property is guaranteed if the eigenfunctions $\hat{\Phi}(s, ik)$ remain unchanged. That is, we posit a *solution* within the layer of the form:

$$[\hat{u}(s, ik, x), \hat{v}(s, ik, x)]^T = \exp\left(\frac{r(s,k)\lambda - \sigma q(s,k)}{r(s,k) + \sigma p(s,k)} x\right) \hat{\Phi}(s, ik),$$

where $\lambda$ and $\Phi$ satisfy (2.3) and $p$, $q$, and $r$ are polynomials in $s$ and $k$. The layer *equations* themselves are directly obtained for any choice of these polynomials by enforcing (2.3).

The central step in the construction of a PML for a particular hyperbolic problem is how to choose the modification of $\lambda$ so that the PML equations remain stable in time. In this paper we will circumvent that issue by looking at two linear hyperbolic-parabolic applications for which it is known that there exist stable PMLs for the corresponding hyperbolic problems. For the hyperbolic-parabolic problem we will use the same modification as would be used for to the hyperbolic problem, taking the point of view that the parabolic terms should, if anything, improve the stability. This standpoint is supported by the fact that we can prove that the PML is stable for the first application. For the second application we do not have any theoretical stability results, but long-time numerical simulations do indicate that the PML is stable.

**2.1. Construction of the general PML model.** Turning to the construction of a PML model for (2.1)–(2.2), we start by introducing the auxiliary variable $w = C_1 \frac{\partial u}{\partial x}$. By reformulating (2.1)–(2.2) in terms of $u, v$, and $w$, a set of first order equations in $x$ is obtained:

$$\underbrace{\begin{bmatrix} \frac{\partial}{\partial t} I - \frac{\partial}{\partial y} B_{11} - \frac{\partial^2}{\partial y^2} C_3 & 0 & -\frac{\partial}{\partial y} B_{12} \\ 0 & I & 0 \\ -\frac{\partial}{\partial y} B_{12}^T & -A_{12}^T C_1^{-1} & \frac{\partial}{\partial t} I - \frac{\partial}{\partial y} B_{22} \end{bmatrix}}_{L} W = \underbrace{\begin{bmatrix} A_{11} + \frac{\partial}{\partial y} C_2 & I & A_{12} \\ C_1 & 0 & 0 \\ 0 & 0 & A_{22} \end{bmatrix}}_{\tilde{A}} \frac{\partial W}{\partial x}. \tag{2.4}$$

Here $W = [u, w, v]^T$. Following the construction of our PML model for hyperbolic systems (described in [5]), we now postulate a PML model for the hyperbolic-parabolic system (2.4). Precisely, we impose the transformation

$$\lambda \to \frac{r(s,k)\lambda - \sigma q(s,k)}{r(s,k) + \sigma p(s,k)}, \tag{2.5}$$

where the polynomials $r$, $p$, and $q$ are defined up to a constant multiple by

$$\chi + \frac{\gamma}{s + \sigma + \beta + ik\alpha} = \frac{p(s,k)}{r(s,k)}, \tag{2.6}$$

$$ik\xi + \mu + \frac{ik\delta + \nu}{s + \sigma + \beta + ik\alpha} = \frac{q(s,k)}{r(s,k)}. \tag{2.7}$$

This leads to the layer equations

$$L\left(\frac{\partial}{\partial t},\frac{\partial}{\partial y},\frac{\partial^2}{\partial y^2}\right)W=\tilde{A}\left((1+\sigma\chi)\frac{\partial W}{\partial x}+\sigma\left(\xi\frac{\partial W}{\partial y}+\mu W+\Phi\right)\right),$$
$$\frac{\partial\Phi}{\partial t}+\alpha\frac{\partial\Phi}{\partial y}+(\sigma+\beta)\Phi=\left(\gamma\frac{\partial W}{\partial x}+\delta\frac{\partial W}{\partial y}+\nu W\right),$$
$$\Phi=\left[\phi^{(u)},\varphi,\phi^{(v)}\right]^T.$$

Or, written out,

(2.8)
$$\frac{\partial u}{\partial t}=\left(A_{11}+\frac{\partial}{\partial y}C_2\right)\left((1+\sigma\chi)\frac{\partial u}{\partial x}+\sigma\left(\xi\frac{\partial u}{\partial y}+\mu u+\phi^{(u)}\right)\right)+B_{11}\frac{\partial u}{\partial y}+B_{12}\frac{\partial v}{\partial y}$$
$$+\left((1+\sigma\chi)\frac{\partial w}{\partial x}+\sigma\left(\xi\frac{\partial w}{\partial y}+\mu w+\varphi\right)\right)+A_{12}\left((1+\sigma\chi)\frac{\partial v}{\partial x}+\sigma\left(\xi\frac{\partial v}{\partial y}+\mu v+\phi^{(v)}\right)\right),$$

(2.9)
$$\frac{\partial v}{\partial t}=A_{22}\left((1+\sigma\chi)\frac{\partial v}{\partial x}+\sigma\left(\xi\frac{\partial v}{\partial y}+\mu v+\phi^{(v)}\right)\right)+A_{12}^T w+B_{22}\frac{\partial v}{\partial y}+B_{12}^T\frac{\partial u}{\partial y},$$

(2.10)
$$\frac{\partial\phi^{(u)}}{\partial t}+\alpha\frac{\partial\phi^{(u)}}{\partial y}+(\sigma+\beta)\phi^{(u)}=\gamma\frac{\partial u}{\partial x}+\delta\frac{\partial u}{\partial y}+\nu u,$$

(2.11)
$$\frac{\partial\phi^{(v)}}{\partial t}+\alpha\frac{\partial\phi^{(v)}}{\partial y}+(\sigma+\beta)\phi^{(v)}=\gamma\frac{\partial v}{\partial x}+\delta\frac{\partial v}{\partial y}+\nu v,$$

(2.12)
$$\frac{\partial\varphi}{\partial t}+\alpha\frac{\partial\varphi}{\partial y}+(\sigma+\beta)\varphi=\gamma\frac{\partial w}{\partial x}+\delta\frac{\partial w}{\partial y}+\nu w,$$
$$w=C_1\left((1+\sigma\chi)\frac{\partial u}{\partial x}+\sigma\left(\xi\frac{\partial u}{\partial y}+\mu u+\phi^{(u)}\right)\right).$$

The parameters $\alpha,\beta,\gamma,\xi,\sigma,\mu$, and $\chi$ are real, and it is assumed that

(2.13)
$$1+\sigma\chi>0.$$

The damping of propagating waves is controlled by $\sigma$ and the damping of evanescent waves by $\beta$ and $\chi$. The other parameters can be used to make adjustments based on the system (2.4) so that the PML model is stable (see also [5, 4]).

*Remark.* We note that the above formulation could easily be extended to any number of space dimensions and to include even more auxiliary functions in the same way as for hyperbolic systems; see [5].

**2.2. Perfect matching property of the general model.** To establish the perfect matching of (2.4) to (2.8)–(2.12) we will construct two solutions. The first solution, denoted by $W_1$, satisfies (2.4) in $\mathbb{R}^2$. The second solution, denoted by $W_2$, satisfies (2.4) in $x<0$ and (2.8)–(2.12) in $x>0$. If the solutions are identical in $x<0$, then the layer is perfectly matched.

Performing a Laplace transform in time and a Fourier transform in $y$ of (2.4), we obtain

(2.14)
$$A\frac{d\hat{W}_1}{dx}=B\hat{W}_1-\hat{W}_0,$$

where $A = \tilde{A}(ik)$ and $B = L(s, ik, -k^2)$ are given by

$$A = \begin{pmatrix} A_{11} + ikC_2 & I & A_{12} \\ C_1 & 0 & 0 \\ 0 & 0 & A_{22} \end{pmatrix}, \quad B = \begin{pmatrix} sI - ikB_{11} + k^2 C_3 & 0 & -ikB_{12} \\ 0 & I & 0 \\ -ikB_{12}^T & -A_{12}^T C_1^{-1} & sI - ikB_{22} \end{pmatrix}.$$

Here $\hat{W}_0 = [\hat{u}_0, 0, \hat{v}_0]^T$, with $\hat{u}_0$, $\hat{v}_0$ being the initial data, and $(s, k)$ are the duals of $(t, y)$.

The solution of (2.14) follows from the solution to the eigenvalue problem

$$\lambda A \xi = B \xi, \tag{2.15}$$

for which we have the following lemma.

LEMMA 2.1. *For $\Re s > 0$ the real parts of the eigenvalues $\lambda$ of the eigenvalue problem* (2.15) *cannot vanish.*

*Proof.* Assume that an eigenvalue was purely imaginary, i.e., $\lambda = i\kappa$, $\kappa \in \mathbb{R}$, and let $\xi = [\xi_u, \xi_w, \xi_v]$, $\xi_u, \xi_w \in \mathbb{C}^p$, $\xi_v \in \mathbb{C}^q$. Then a direct computation of $\Re\{\xi^*(\lambda A - B)\xi\}$ gives the contradiction

$$\Re s + \frac{\xi_u^* \left(k^2 C_3 + \kappa k C_2 + |\kappa|^2 C_1\right) \xi_u}{|\xi_u|^2 + |\xi_v|^2} = 0,$$

by assumption (A3). ∎

Lemma 2.1 allows us to order the eigenvalues of (2.15) into two sets labeled by the sign of their real parts

$$\Re\lambda_1, \ldots, \Re\lambda_r < 0, \tag{2.16}$$

$$\Re\lambda_{r+1}, \ldots, \Re\lambda_{2p+q} > 0. \tag{2.17}$$

Here $r = p + r_2$, where $r_2$ is the number of negative eigenvalues of $A_{22}$. This follows from the study of the eigenvalue problem for $\Re s \gg 1 + k^2$. Precisely, if $(\gamma_j, P_j)$, $j = 1, \ldots, p$, are eigenpairs of $C_1$ and $(\sigma_j, Q_j)$, $j = 1, \ldots, q$, are eigenpairs for $A_{22}$, then

$$\left( \pm \left( \frac{s}{\gamma_j} \right)^{1/2}, \begin{pmatrix} \pm(s\gamma_j)^{-1/2} P_j \\ P_j \\ 0 \end{pmatrix} \right), \quad \left( \frac{s}{\sigma_j}, \begin{pmatrix} 0 \\ 0 \\ Q_j \end{pmatrix} \right) \tag{2.18}$$

are approximate solutions of (2.15).

To write down the solution of (2.14) we use the matrix

$$M(s, k) = A(s, k)^{-1} B(s, k),$$

where the existence of $A^{-1}$ is guaranteed by assumptions (A2) and (A3). Further, there exists a matrix $Q$ that block diagonalizes $M(s, k)$:

$$QMQ^{-1} = \begin{bmatrix} S^- & 0 \\ 0 & S^+ \end{bmatrix},$$

where the eigenvalues (2.16) are the eigenvalues of $S^-$ and the eigenvalues (2.17) are the eigenvalues of $S^+$. The bounded solution of (2.14) is now easy to write down:

$$\hat{W}_1 = Q^{-1} \begin{pmatrix} \int_{-\infty}^{x} e^{S^-(x-y)} f^-(y) dy \\ -\int_{x}^{\infty} e^{S^+(x-y)} f^+(y) dy \end{pmatrix}, \tag{2.19}$$

where

$$-QA^{-1}\hat{W}_0 = \begin{pmatrix} f^- \\ f^+ \end{pmatrix}. \tag{2.20}$$

Note that the support properties of $\hat{W}_0$ and thus $f^{\pm}$ guarantees the existence of the integrals in (2.19) and that at $x = 0$:

$$\hat{W}_1 = Q^{-1} \begin{pmatrix} \int_{-H}^{-h} e^{-S^- y} f^-(y) dy \\ 0 \end{pmatrix}. \tag{2.21}$$

We now construct solutions to the second problem. For $x < 0$ the governing equations are

$$A \frac{d\hat{W}_2^L}{dx} = B\hat{W}_2^L - \hat{W}_0, \tag{2.22}$$

and for $x > 0$

$$A\left((1+\sigma\chi)\frac{d\hat{W}_2^R}{dx} + \sigma\left(ik\xi\hat{W}_2^R + \mu\hat{W}_2^R\right) + \sigma\hat{\Phi}\right) = B\hat{W}_2^R, \tag{2.23}$$

$$s\hat{\Phi} + ik\alpha\hat{\Phi} + (\sigma+\beta)\hat{\Phi} = \gamma\frac{d\hat{W}_2^R}{dx} + ik\delta\hat{W}_2^R + \nu\hat{W}_2^R. \tag{2.24}$$

We compute $\hat{W}_2$ in each region, noting first that (2.24) can be solved directly:

$$\hat{\Phi} = \frac{\gamma\frac{d\hat{W}_2^R}{dx} + (ik\delta+\nu)\hat{W}_2^R}{s+\sigma+\beta+ik\alpha}. \tag{2.25}$$

For $x > 0$ we transform the solution using the same transformation $Q$ which block diagonalizes the problem for $x < 0$. Setting $\hat{V} = Q\hat{W}_2^R$, we find

$$\frac{d\hat{V}}{dx} = \frac{1}{r(s,k)+\sigma p(s,k)} \begin{pmatrix} r(s,k)S^- - \sigma q(s,k)I & 0 \\ 0 & r(s,k)S^+ - \sigma q(s,k)I \end{pmatrix} \hat{V}, \tag{2.26}$$

where $p$, $q$, and $r$ were specified in (2.6)–(2.7). From the limits

$$\lim_{|s|\to\infty} \frac{p}{r} = \chi, \qquad \lim_{|s|\to\infty} \frac{q}{r} = ik\xi + \mu, \tag{2.27}$$

it follows that for large $s$ the eigenvalues of the blocks of (2.26) are approximately

$$\frac{\lambda_j - \sigma(ik\xi+\mu)}{1+\sigma\chi}. \tag{2.28}$$

From (2.18) and (2.13), we conclude that if we choose $\Re s$ sufficiently large, the signs of the real part of the eigenvalues of the blocks of (2.26) are the same as the signs of $\Re\lambda_j$. The transform of the causal solution $\hat{W}_2$ in $x > 0$ takes the form

$$\hat{W}_2^R = Q^{-1} \begin{pmatrix} e^{(r+\sigma p)^{-1}(rS^- - \sigma qI)x}\hat{V}^- \\ 0 \end{pmatrix}. \tag{2.29}$$

We see that $\hat{W}_2$ can be "perfectly matched" to the restriction of $\hat{W}_1$ to $x < 0$ by setting

$$\hat{V}^- = \int_{-H}^{-h} e^{-S^- y} f^-(y) dy. \tag{2.30}$$

Thus we have proved that $W_1$ and $W_2$ restricted to $x < 0$ are identical and that our PML model is perfectly matched.

**3. Applications.** In this section we present two linear and one nonlinear application of our general PML model.

**3.1. The wave equation with parabolic damping.** We first consider the application of our model to the linear wave equation in two dimensions with a parabolic damping term

$$\frac{\partial^2 u}{\partial t^2} - \frac{\partial^2 u}{\partial x^2} - \frac{\partial^2 u}{\partial y^2} = \varepsilon \left( \frac{\partial^3 u}{\partial t \partial x^2} + \frac{\partial^3 u}{\partial t \partial y^2} \right) \tag{3.1}$$

on $(x, y) \in \mathbb{R}^2$, with initial data

$$u(0, x, u) = u_0(x, y), \qquad \frac{\partial u(0, x, u)}{\partial t} = u_1(x, y).$$

By introducing $v = u_t$, $w = u_x$, and $p = u_y$, (3.1) can be written as the following first order mixed system:

$$\begin{aligned} \frac{\partial v}{\partial t} &= \frac{\partial w}{\partial x} + \frac{\partial p}{\partial y} + \varepsilon \left( \frac{\partial^2 v}{\partial x^2} + \frac{\partial^2 v}{\partial y^2} \right), \\ \frac{\partial w}{\partial t} &= \frac{\partial v}{\partial x}, \\ \frac{\partial p}{\partial t} &= \frac{\partial v}{\partial y}, \end{aligned} \tag{3.2}$$

with initial data

$$v(0, x, y) = u_1(x, y), \quad w(0, x, y) = \frac{\partial u_0(x, y)}{\partial x}, \quad p(0, x, y) = \frac{\partial u_0(x, y)}{\partial y}.$$

First, consider a layer in the $x$ direction. As there is no derivative of $p$ with respect to $x$ in (3.2), we need only to apply the hyperbolic damping functions to $v$ and $w$. Similarly, we apply only the parabolic damping to $v$, as $v_{xx}$ is the only parabolic term. The hyperbolic problem obtained when $\varepsilon = 0$ is equivalent to Maxwell's equations, and we know from our previous work on general formulations for hyperbolic systems [4] that suitable choices of parameters in the PML are $\xi, \mu, \alpha, \delta, \mu = 0$, $\gamma = -1$, and

$\beta \geq 0$. With these choices, we get the following equations in the layer:

$$
\begin{aligned}
\frac{\partial v}{\partial t} =& \frac{\partial w}{\partial x} + \sigma_x \phi_x^{(w)} + \frac{\partial p}{\partial y} \\
&+ \varepsilon \left( \frac{\partial^2 v}{\partial x^2} + \frac{\partial^2 v}{\partial y^2} + \frac{\partial \left( \sigma_x \phi_x^{(v)} \right)}{\partial x} + \sigma_x \varphi_x^{(v)} \right), \\
\frac{\partial w}{\partial t} =& \frac{\partial v}{\partial x} + \sigma_x \phi_x^{(v)}, \\
\frac{\partial p}{\partial t} =& \frac{\partial v}{\partial y}, \\
\frac{\partial \phi_x^{(v)}}{\partial t} + (\sigma_x + \beta)\phi_x^{(v)} =& - \frac{\partial v}{\partial x}, \\
\frac{\partial \phi_x^{(w)}}{\partial t} + (\sigma_x + \beta)\phi_x^{(w)} =& - \frac{\partial w}{\partial x}, \\
\frac{\partial \varphi_x^{(v)}}{\partial t} + (\sigma_x + \beta)\varphi_x^{(v)} =& - \left( \frac{\partial^2 v}{\partial x^2} + \frac{\partial \left( \sigma_x \phi^{(v)} \right)}{\partial x} \right).
\end{aligned}
\tag{3.3}
$$

**3.1.1. Stability.** For constant damping, $\sigma_x = \text{const} > 0$ and $\beta = 0$, we perform a Fourier transform in space (the duals of $(x, y)$ are $(k_x, k_y)$) of (3.3) and obtain

$$
\frac{d\hat{U}}{dt} = P(ik_x, ik_y)\hat{U},
$$

where $U = [v, w, p, \phi_x^{(v)}, \phi_x^{(w)}, \varphi_x^{(v)}]^T$. The eigenvalues of the symbol $P(ik_x, ik_y)$ are the roots of the characteristic polynomial

$$
\det(\lambda I - P) = \lambda(\lambda + \sigma_x) q(\lambda) = 0,
$$

where

$$
\begin{aligned}
q(\lambda) = \lambda^4 + \left(2\sigma_x + \varepsilon k_x^2 + \varepsilon k_y^2\right)\lambda^3 + \left(\sigma_x^2 + 2\varepsilon\sigma_x k_y^2 + k_x^2 + k_y^2\right)\lambda^2 \\
+ \left(\varepsilon\sigma_x^2 k_y^2 + 2\sigma_x k_y^2\right)\lambda + \sigma_x^2 k_y^2,
\end{aligned}
\tag{3.4}
$$

and the sign of their real part determines the stability of the PML model. Obviously for $k_y \neq 0$ the single zero eigenvalue and the eigenvalue $\lambda = -\sigma_x$ will not cause instability, and it remains only to check that the roots of $q(\lambda)$ have negative real part. To check this we use the following lemma.

LEMMA 3.1 (Lemma 6 in [5]). *Consider any polynomial $q(\lambda)$ of degree $n$. Let $D$ be a real number, and define the polynomials $Q_0$ and $Q_1$ with real coefficients by*

$$
q(iD) \equiv i^n \left[ Q_0(D) + iQ_1(D) \right].
\tag{3.5}
$$

*Then there is a continued fraction*

$$
\frac{Q_1(D)}{Q_0(D)} = \cfrac{1}{c_1 D + d_1 - \cfrac{1}{c_2 D + d_2 - \cfrac{1}{c_3 D + d_3 - \cdots - \cfrac{1}{c_{n_r} D + d_{n_r}}}}},
\tag{3.6}
$$

*with $c_j \neq 0$ and $n_r \leq n$. The number of roots with positive (negative) real part equals the number of positive (negative) $c_j$. There are $n - n_r$ roots on the imaginary axis.*

For the $q(\lambda)$ defined in (3.4) we get

$$c_1 = -\frac{1}{l_1}, \quad c_2 = -\frac{l_1^2}{l_2}, \quad c_3 = -\frac{l_2^2}{\sigma_x k_y^2 l_1}, \quad c_4 = -\frac{l_3}{\sigma_x l_2}, \tag{3.7}$$

where

$$\begin{aligned}
l_1 &= \varepsilon\left(k_x^2 + k_y^2\right) + 2\sigma_x, \\
l_2 &= 2\sigma_x\left(k_x^2 + \sigma_x^2\right) + \varepsilon\left(\left(k_x^2 + k_y^2\right)^2 + \sigma_x^2\left(k_x^2 + 4k_y^2\right)\right) + \varepsilon^2\left(2\sigma k_y^2\left(k_x^2 + k_y^2\right)\right), \\
l_3 &= k_y^4 2\varepsilon(\varepsilon\sigma_x + 1)^2 + k_y^2 2\varepsilon\left(2\varepsilon k_y^2\sigma_x + \varepsilon^2\sigma_x^2 k_y^2 + 2\varepsilon\sigma_x^3 + 2k_x^2 + 2\sigma_x^2\right) \\
&\quad + \left(\varepsilon k_y^2 + 2\sigma_x\right)\left(\varepsilon\sigma_x^3 + 2k_y^2\right).
\end{aligned}$$

For $k_y \neq 0$ it is clear that $c_j < 0$, $j = 1, \ldots, 4$, and thus the roots have negative real part. Finally, if $k_y = 0$, two roots of $q$ have negative real part and zero is a double root. Then we must check the triple eigenvalue $\lambda = 0$. We find three independent null vectors: $[\sigma_x, 0, 0, -ik_x, 0, 0]^T$, $[0, \sigma_x, 0, 0, -ik_x, 0, 0]^T$, $[0, 0, 1, 0, 0, 0]^T$. Thus the PML model is stable. Note also that by the techniques described in [16, 5], we automatically get an energy estimate from (3.7).

**3.1.2. A numerical experiment.** To test the performance of our model, we solve (3.2) on the domain $(x, y) \in [-5, 5] \times [-5, 5]$ with the initial data

$$u_0(x, y) = \exp\left(-\left(x^2 + y^2\right)\right), \qquad u_1(x, y) = 0.$$

Inside the computational domain we solve (3.2). To truncate the computational domain we add layers of width 1 to all sides. In the layers, (A.1)–(A.9) are solved. The layers are terminated with periodic boundary conditions.

The equations are discretized with standard 8th order accurate centered finite differences (using grid spacing 0.1) in space and with an 8th order accurate 12 stage Runge–Kutta method [29] in time.

As we use a high order method, the damping functions $\sigma_z(z), z = x, y$, should be sufficiently smooth at the interface between the computational domain and the PML and at the end of the layer (recall that we use periodic boundary conditions). For this problem we choose the damping functions to be

$$\sigma_z(z) = \begin{cases} \sigma_{\max}\left(1 - (|z| - 5)^2\right)^8 & 5 \leq |z| \leq 6, \\ 0 & \text{everywhere else,} \end{cases}$$

where the maximum damping $\sigma_{\max}$ has been chosen empirically to 10.

To assess the performance of the PML for hyperbolic-parabolic systems, we implemented the standard PML that would be used for the undamped wave equation (specifically, the standard PML is obtained by setting $\varphi_x^{(v)}$ and $\varphi_y^{(v)}$ to zero in (A.1)–

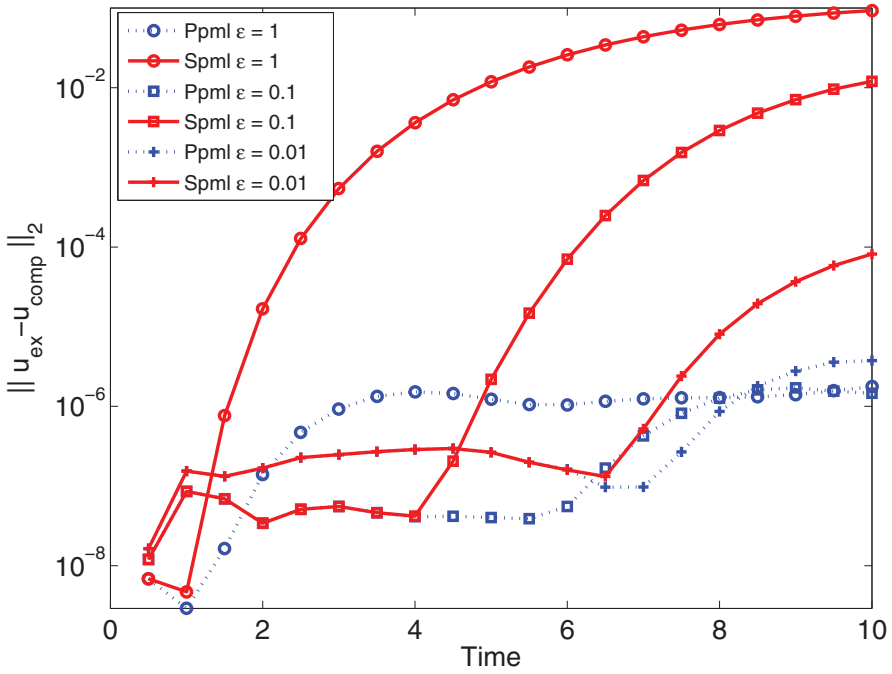


FIG. 3.1. *Comparison between our parabolic PML (Ppml in the legend) and the PML for the undamped system (Spml in the legend).*

(A.9)). Using these models the computed solutions are compared to an "exact" solution, which we obtain by first solving the ordinary differential equation

$$\frac{d^2\hat{u}}{dt^2} + \varepsilon\left(k_x^2 + k_y^2\right)\frac{d\hat{u}}{dt} + \left(k_x^2 + k_y^2\right)\hat{u} = 0, \tag{3.8}$$

$$\hat{u}(0, k_x, k_y) = \hat{u}_0(k_x, k_y), \qquad \frac{du(0, \hat{k_x}, k_y)}{dt} = \hat{u}_1(k_x, k_y),$$

resulting from taking the Fourier transform in space of (3.1). The "exact" solution is then computed by using the solution of (3.8) to evolve the Fourier transformed initial data $\hat{u}_0, \hat{u}_1$ and finally computing the inverse Fourier transform numerically.

In Figure 3.1 the $l^2$-norm (taken over the computational domain) of the absolute error between the "exact" solution and the computed solutions, for different values of $\varepsilon$, are plotted as a function of time. From the plot it is clear that the performance of the suggested PML is much better than the PML designed for purely hyperbolic problems. It is also evident from the curve corresponding to $\varepsilon = 0.1$ that the perfect matching property is lost when the standard PML is used; the time at which the first wave passes out of the computational domain coincides with the time the error rises. At this time the error from the proposed PML is lower and rises only later. The rise starts approximately two time units later, a time that coincides with the time it takes for the wave front to pass through the layer without any reflection.

**3.2. A PML model for the compressible Navier–Stokes equations linearized around parallel flow.** Our second application is the linearized Navier–

TABLE 3.1
*Variables and constants.*

| | |
|---|---|
| $\rho$ | density |
| $u = (u_1, u_2)^T$ | velocity vector |
| $T$ | temperature |
| $\gamma$ | ratio of specific heats |
| Pr | Prandtl number |
| $L$ | characteristic length |
| $\rho_\infty$ | mean density |
| $u_\infty$ | mean velocity |
| Re | Reynolds number |
| $\frac{D}{Dt}$ | substantial derivative |

Stokes equations, which are derived from the compressible Navier–Stokes equations

$$\frac{\partial \rho}{\partial t} + u \cdot \nabla \rho + \rho(\nabla \cdot u) = 0, \tag{3.9}$$

$$\frac{Du_1}{Dt} + \frac{T}{\rho}\frac{\partial \rho}{\partial x_1} + \frac{\partial T}{\partial x_1} = \frac{1}{\mathrm{Re}\rho}\left(\frac{4}{3}\frac{\partial^2 u_1}{\partial x_1^2} + \frac{\partial^2 u_1}{\partial x_2^2} + \frac{1}{3}\frac{\partial^2 u_2}{\partial x_1 \partial x_2}\right), \tag{3.10}$$

$$\frac{Du_2}{Dt} + \frac{T}{\rho}\frac{\partial \rho}{\partial x_2} + \frac{\partial T}{\partial x_2} = \frac{1}{\mathrm{Re}\rho}\left(\frac{4}{3}\frac{\partial^2 u_2}{\partial x_2^2} + \frac{\partial^2 u_2}{\partial x_1^2} + \frac{1}{3}\frac{\partial^2 u_1}{\partial x_1 \partial x_2}\right), \tag{3.11}$$

$$\begin{aligned}\frac{DT}{Dt} + (\gamma - 1)T\left(\frac{\partial u_1}{\partial x_1} + \frac{\partial u_2}{\partial x_2}\right) &= \frac{\gamma}{\rho \mathrm{RePr}}\left(\frac{\partial^2 T}{\partial x_1^2} + \frac{\partial^2 T}{\partial x_2^2}\right) \\ &+ \frac{\gamma - 1}{\rho \mathrm{Re}}\left(\frac{4}{3}\left[\left(\frac{\partial u_1}{\partial x_1}\right)^2 + \left(\frac{\partial u_2}{\partial x_2}\right)^2 - \frac{\partial u_1}{\partial x_1}\frac{\partial u_2}{\partial x_2}\right] + \left(\frac{\partial u_1}{\partial x_2} + \frac{\partial u_2}{\partial x_1}\right)^2\right).\end{aligned} \tag{3.12}$$

We have assumed that the fluid is Newtonian and obeys the ideal gas law; we have also nondimensionalized the equations using the scalings

$$\tilde{t} = \frac{L}{u_\infty}t, \quad \tilde{x} = Lx, \quad \tilde{\rho} = \rho_\infty \rho, \quad \tilde{u}_1 = u_\infty u_1, \quad \tilde{u}_2 = u_\infty u_2, \quad \tilde{T} = \frac{u_\infty^2}{\mathrm{Re}}T.$$

Here the dimensional variables are marked by a tilde, and the other quantities appearing in the above equations are detailed in Table 3.1.

The linearized equations are obtained by considering perturbations $(\rho', u_1', u_2', T')$ around a mean flow $(\bar{\rho}, \bar{u}_1, \bar{u}_2, \bar{T})$. Substituting

$$\rho = \bar{\rho} + \rho', \quad u_1 = M_1 + u_1', \quad u_2 = M_2 + u_2', \quad T = \bar{T} + T', \tag{3.13}$$

into (3.9)–(3.12) and neglecting higher order terms, we arrive at the linearized Navier–Stokes equations (we have dropped the primes)

$$\begin{aligned}
&\frac{\partial \rho}{\partial t} + M_1\frac{\partial \rho}{\partial x_1} + M_2\frac{\partial \rho}{\partial x_2} + \bar{\rho}(\nabla \cdot u) = 0, \\
&\frac{\partial u_1}{\partial t} + M_1\frac{\partial u_1}{\partial x_1} + M_2\frac{\partial u_1}{\partial x_2} + \frac{\bar{T}}{\bar{\rho}}\frac{\partial \rho}{\partial x_1} + \frac{\partial T}{\partial x_1} = \frac{1}{\mathrm{Re}\bar{\rho}}\left(\frac{4}{3}\frac{\partial^2 u_1}{\partial x_1^2} + \frac{\partial^2 u_1}{\partial x_2^2} + \frac{1}{3}\frac{\partial^2 u_2}{\partial x_1 \partial x_2}\right), \\
&\frac{\partial u_2}{\partial t} + M_1\frac{\partial u_2}{\partial x_1} + M_2\frac{\partial u_2}{\partial x_2} + \frac{\bar{T}}{\bar{\rho}}\frac{\partial \rho}{\partial x_2} + \frac{\partial T}{\partial x_2} = \frac{1}{\mathrm{Re}\bar{\rho}}\left(\frac{4}{3}\frac{\partial^2 u_2}{\partial x_2^2} + \frac{\partial^2 u_2}{\partial x_1^2} + \frac{1}{3}\frac{\partial^2 u_1}{\partial x_1 \partial x_2}\right), \\
&\frac{\partial T}{\partial t} + M_1\frac{\partial T}{\partial x_1} + M_2\frac{\partial T}{\partial x_2} + (\gamma - 1)\bar{T}\left(\frac{\partial u_1}{\partial x_1} + \frac{\partial u_2}{\partial x_2}\right) = \frac{\gamma}{\bar{\rho}\mathrm{RePr}}\left(\frac{\partial^2 T}{\partial x_1^2} + \frac{\partial^2 T}{\partial x_2^2}\right).
\end{aligned}$$

Based on knowledge from previous work on the linearized Euler equations (see, e.g., [5]) we propose the following layer for a uniform flow aligned with the $x$-axis $((\bar{\rho}, \bar{u}_1, \bar{u}_2, \bar{T}) = (\bar{\rho}, M_1, 0, \bar{T}))$:

$$\frac{\partial \rho}{\partial t} + M_1 r^{(\rho)} + \bar{\rho} r^{(u_1)} + \bar{\rho} \frac{\partial u_2}{\partial x_2} = 0, \tag{3.14}$$

$$\frac{\partial u_1}{\partial t} + M_1 r^{(u_1)} + \frac{\bar{T}}{\bar{\rho}} r^{(\rho)} + r^{(T)} = \frac{1}{\mathrm{Re}\bar{\rho}} \left[ \frac{4}{3} q^{(u_1)} + \frac{\partial^2 u_1}{\partial x_2^2} + \frac{1}{3} \frac{\partial r^{(u_2)}}{\partial x_2} \right], \tag{3.15}$$

$$\frac{\partial u_2}{\partial t} + M_1 r^{(u_2)} + \frac{\bar{T}}{\bar{\rho}} \frac{\partial \rho}{\partial x_2} + \frac{\partial T}{\partial x_2} = \frac{1}{\mathrm{Re}\bar{\rho}} \left[ q^{(u_2)} + \frac{4}{3} \frac{\partial^2 u_2}{\partial x_2^2} + \frac{1}{3} \frac{\partial r^{(u_1)}}{\partial x_2} \right], \tag{3.16}$$

$$\frac{\partial T}{\partial t} + M_1 r^{(T)} + (\gamma - 1)\bar{T} r^{(u_1)} + (\gamma - 1)\bar{T} \frac{\partial u_2}{\partial x_2} = \frac{\gamma}{\mathrm{RePr}\bar{\rho}} \left[ q^{(T)} + \frac{\partial^2 T}{\partial x_2^2} \right], \tag{3.17}$$

$$\frac{\partial \phi^{(l)}}{\partial t} + \left( \eta \frac{\partial l}{\partial x_1} + (\sigma + \alpha) \left( \mu l + \phi^{(l)} \right) \right) = 0, \qquad l = \rho, u_1, u_2, T, \tag{3.18}$$

$$\frac{\partial \varphi^{(l)}}{\partial t} + \left[ w^{(l)} + (\sigma + \alpha) \left( \mu r^{(l)} + \varphi^{(l)} \right) \right] = 0, \qquad l = u_1, u_2, T. \tag{3.19}$$

Here the index $l$ implies that there is an equation for each $l$, e.g., (3.18) is to be interpreted as four equations. The auxiliary variables $r, w$, and $q$ are

$$r^{(l)} \equiv \left( \eta \frac{\partial l}{\partial x_1} + \sigma \left( \mu l + \phi^{(l)} \right) \right), \qquad l = \rho, u_1, u_2, T,$$

$$w^{(l)} \equiv \eta^2 \frac{\partial^2 l}{\partial x_1^2} + \left( \frac{\partial \eta}{\partial x_1} + \sigma\mu \right) \eta \frac{\partial l}{\partial x_1} + \sigma \frac{\partial \phi^{(l)}}{\partial x_1} + \eta \frac{\partial \sigma}{\partial x_1} \left( \mu l + \phi^{(l)} \right), \qquad l = u_1, u_2, T,$$

$$q^{(l)} \equiv w^{(l)} + \sigma \left( \mu r^{(l)} + \varphi^{(l)} \right), \qquad l = u_1, u_2, T.$$

Note that by setting $\varphi^{(l)} \equiv 0$, we recover a PML for the linearized Euler equations. Note also that we have replaced the notation for the stretching function $(1 + \sigma\chi)$ by $\eta \equiv 1 + \sigma\chi$.

**3.2.1. A numerical experiment: Effects of the damping parameters for a continuously forced problem.** To test the performance of our PML model we discretize (3.14)–(3.19) on a Cartesian grid covering the the domain $(x, y) \in [-(10 + L_{lay}), 10 + L_{lay}] \times [-10, 10]$. The computational domain consists of the inner $20 \times 20$ domain excluding the layers of width $L_{lay}$ added at the end. We use periodic boundary conditions both to truncate the computational domain in the $y$-direction and to truncate the layers in the $x$-direction. For all experiments we choose the damping function to be

$$\sigma(x) = \begin{cases} \sigma_{\max} \left( 1 - \left( \frac{|x| - 10}{L_{lay}} \right)^2 \right)^8 & 10 \le |x| \le 10 + L_{lay}, \\ 0 & \text{else}, \end{cases}$$

and the stretching function $\eta$ to be

$$\eta(x) = \begin{cases} \left(1 + \eta_{\max}\left(1 - \left(\frac{|x|-10}{L_{lay}}\right)^2\right)^8\right)^{-1} & 10 \le |x| \le 10 + L_{lay}, \\ 1 & \text{else.} \end{cases}$$

All spatial derivatives are approximated by standard eighth order centered finite differences. In time we use the same eighth order Runge–Kutta method as in the previous section. For all computations in this section we take the grid size to be 0.02, and the time step is chosen close to the stability limit for the problem without the PML.

The mean flow is taken to be $\bar{\rho} = 1, M_1 = 0.1, M_2 = 0, \bar{T} = \gamma^{-1}$, and the Reynolds number, the Prandtl number, and ratio of specific heats are taken to be

$$\mathrm{Re} = 1000, \quad \mathrm{Pr} = 0.7, \quad \gamma = \frac{5}{3}.$$

For the corresponding hyperbolic PML to be stable we must choose (see, e.g., [5])

$$\mu = \frac{M_1}{1 - M_1^2}. \tag{3.20}$$

We make the same choice for our model where viscosity is included, but note that this is only guaranteed to give stability in the limit of no viscosity; see also section 3.2.2 below.

We take the initial data to be zero and continuously force the right-hand side of (3.14), (3.15), and (3.16) by

$$\begin{aligned} f_1 &= \sin\frac{\pi t}{3}\exp\left(-\log 2\,\left((x-3)^2 + y^2\right)\right), \\ f_2 &= 0.5y\sin\frac{\pi t}{2}\exp\left(-\log 2\,\left((x+3)^2 + y^2\right)\right), \\ f_3 &= -0.5x\sin\frac{\pi t}{2}\exp\left(-\log 2\,\left((x+3)^2 + y^2\right)\right). \end{aligned}$$

For a fixed final time, fixed wave number content, and with $\eta = 0$, it is expected (from the theory for hyperbolic PMLs) that the continuous error from a PML of width $L_{lay}$ and maximum strength $\sigma_{\max}$ behave as

$$e_{PML} \sim e^{-L_{lay}\sigma_{\max}}. \tag{3.21}$$

For a discretized *perfectly matched* damping layer we expect (3.21) to hold if the damping function $\sigma(x)$ is well resolved, i.e., when $L_{lay}$ is large and $\sigma_{\max}$ is small. If the product $L_{lay}\sigma_{\max}$ is large enough and the damping function is resolved, the error in the computation should be approaching the discretization error of the interior scheme.

On the other hand, for a damping layer without the *perfect matching* property, we expect (both for the continuous and the discrete problem) the main source of error to be direct reflections from the interface of the layer and the computational domain. The amount of the direct reflections depends mainly on the magnitude of the damping function; thus, as $\sigma_{\max}$ become smaller the error decreases. However, as long as $\sigma(x) \neq 0$, there will be an error due to direct reflection; moreover, this error will not decrease as the grid spacing tends to zero.

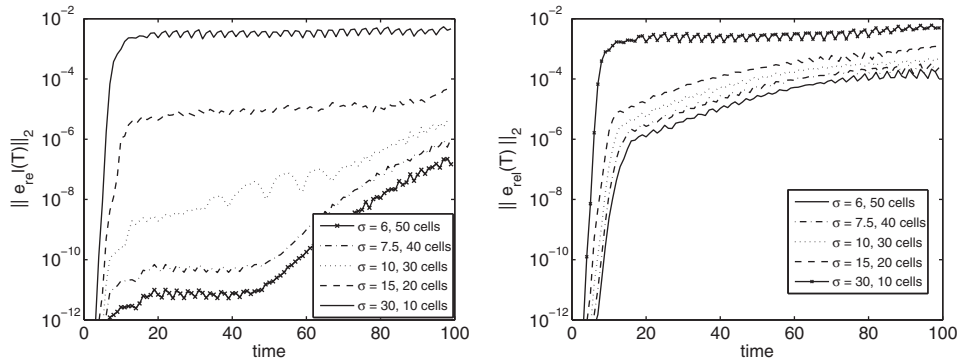


(a) Effects of discretization for the new hyperbolic-parabolic layer.

(b) Results for a hyperbolic PML designed for the linearized Euler equations.

FIG. 3.2. *Comparison of the new layer and a conventional hyperbolic layer. The product* $L_{lay}\sigma_{\max}$ *is kept fixed; thus in the continuous setting the new PML should be equivalently efficient for all widths. However, here we solve a discretized problem, and the performance will depend on how well the damping function in the layer is resolved. Note that the hyperbolic layer is not perfectly matched to the hyperbolic-parabolic equations, and as a result the error levels are many orders of magnitude larger than for the new layer.*

To verify that our model is perfectly matched and to test how much the lack of perfect matching of a conventional hyperbolic layer reduces its accuracy, the following experiment is performed. Fixing $L_{lay}\sigma_{\max} = 300h$ solutions for $L_{lay} = 10h, 20h, 30h, 40h, 50h$ are computed and compared to a reference solution (computed on a much larger domain). The comparison is performed by computing the relative error in the $T$ component (the errors in $\rho, u_1$, and $u_2$ behave similarly) defined as

$$e_{rel}(T) = \left( \frac{\sum_i \sum_j h^2 (T_{i,j} - T_{i,j}^{exact})^2}{\sum_i \sum_j h^2 (T_{i,j}^{exact})^2} \right)^{\frac{1}{2}}.$$

Here the sums are computed over the indicies $i, j$ belonging to gridpoints $(x_i, y_j)$ that are in the computational domain.

In Figure 3.2 the results for the suggested layer are compared to the results obtained using a layer for the corresponding hyperbolic problem (defined by setting $\varphi^{(l)} \equiv 0$). For the thinnest layer (10 grid points wide) the error of the new PML model rises at time $t \approx 4$ when the first waves impinge on the interface between the layer and the computational domain. As the layer is widened, the damping function becomes smaller and better resolved, and the level of the error is reduced drastically. On the other hand, for the hyperbolic layer, the error decreases only marginally as the layer is widened; the perfect matching is lost.

As can be seen in Figure 3.2(a), the error starts to increase at later times ($t \approx 50$). This is in good agreement with the theory in [20], which states that the error should increase with time as

$$e_{PML} \sim C_1 e^{-\frac{C_2}{\sqrt{t}}}. \tag{3.22}$$

In Figure 3.3 we have zoomed in on the error for the computation with the widest layer and fitted (3.22) to the data; the solid fitted line line is $10^6 e^{-240/\sqrt{t}}$. This late time growth is intrinsic for a PML on an equidistant grid, but it can be reduced by

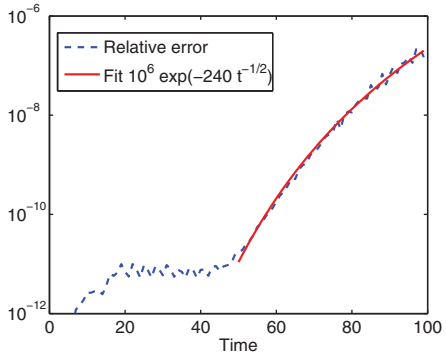


FIG. 3.3. *Fit of the norm of the relative error to* $e^{-240\frac{1}{\sqrt{t}}}$.

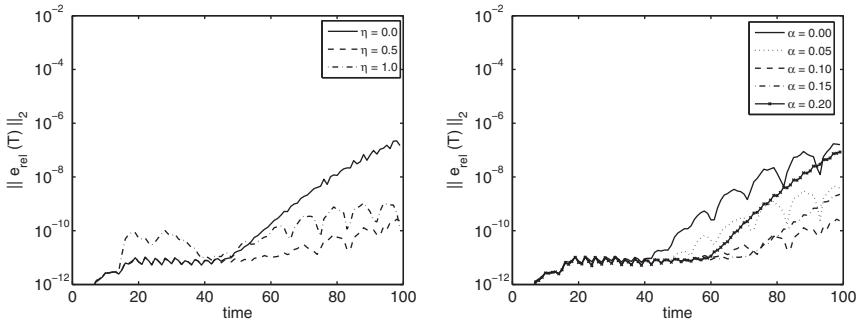


(a) Including $\eta$. (b) Varying $\alpha$.

FIG. 3.4.

invoking the additional damping function $\eta$ that acts as stretching of the grid toward the end of the layer. In Figure 3.4(a) we plot the results for some different values of $\eta_{\max}$ (in these computations we use $\alpha = 0.1$). Clearly the results are improved further by including $\eta$. Finally, in Figure 3.4(b) results for some different values of $\alpha$, keeping $\eta_{\max} = 0.1$ fixed, are plotted. We stress that the best results with the new layer are *6 orders of magnitude* better than the standard PML.

**3.2.2. Stability.** For the PML (3.14)–(3.19) we are not able to establish stability via the characteristic polynomial due to the complexity of the algebriac expressions produced using the Sturm sequences. A partial stability result can be obtained for the special case when $M_1 = 0$; then the characteristic polynomial factors into a first degree, a third degree, and a seventh degree polynomial. For each of these it can be checked that the Sturm sequence conditions hold for constant damping and no stretching, but the expressions are very lengthy and therefore not included here.

To further study the stability of the PML we have performed a series of long time simulations for several values of $M_1$ and Re. We found that the PML is unstable for very small Re and values of $M_1$ close to 1; see Figure 3.5. Recall [5] that the hyperbolic PML is unstable when $M_1 > 1$. As the location of the eigenvalues of the hyperbolic system are perturbed by the viscous term, it is not surprising that the new PML becomes unstable for $M_1$ close to 1 and large viscosity (i.e., small Re).

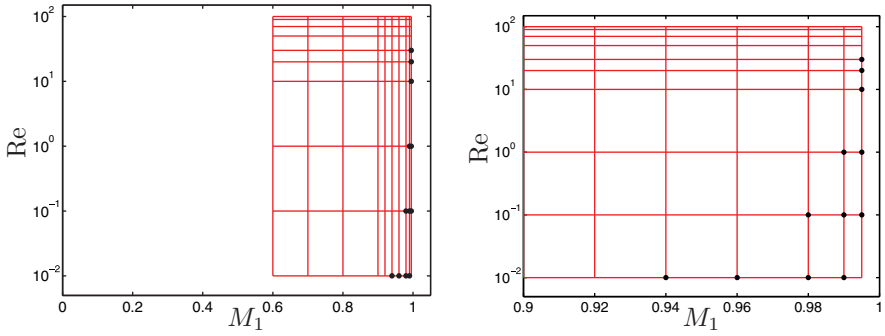


FIG. 3.5. *Long time computations have been performed for values of* $(M_1, Re)$ *at the intersection of the lines. The dots are values that give unstable solutions. The right figure is a zoom in of the left figure for* $0.9 \leq M_1 \leq 1$. *Note that the vertical scale is logarithmic.*

**4. An absorbing layer for the compressible Navier–Stokes equations.** Our final application is the full compressible Navier–Stokes equations (3.9)–(3.12). As for the linearized equations, we consider the case with a parallel mean flow $(\bar{\rho}, \bar{u}_1, \bar{u}_2, \bar{T})$. The main difference in the construction of the damping layer, compared to the linear case, is that the layer cannot be designed to absorb towards zero, but rather towards some fixed state. For this example it is natural to damp towards the mean flow; see also Hu [24]. Choosing to do so, we end up with the following layer model:

$$\frac{D\rho}{Dt} + \rho(\nabla \cdot u) + \rho\sigma(\mu(u_1 - \bar{u}_1) + \phi^{u_1}) + u_1\sigma(\mu(\rho - \bar{\rho}) + \phi^{\rho}) = 0, \tag{4.1}$$

$$\begin{aligned}\frac{Du_1}{Dt} &+ (\gamma - 1)\left(\frac{T}{\rho}\frac{\partial \rho}{\partial x} + \frac{\partial T}{\partial x}\right) + u_1\sigma(\mu(u_1 - \bar{u}_1) + \phi^{u_1}) \\ &+ (\gamma - 1)\frac{T}{\rho}\sigma(\mu(\rho - \bar{\rho}) + \phi^{\rho}) + (\gamma - 1)\sigma\left(\mu\left(T - \bar{T}\right) + \phi^{T}\right) \\ &= \frac{1}{\mathrm{Re}\rho}\left[\frac{4}{3}\left[\eta^2\frac{\partial^2 u_1}{\partial x^2} + (\eta' + \sigma\mu)\eta\frac{\partial u_1}{\partial x} + \sigma\eta\frac{\partial \phi^{u_1}}{\partial x} + \sigma'\eta(\mu(u_1 - \bar{u}_1) + \phi^{u_1})\right.\right. \\ &\left.\left. + \sigma\left(\mu\left(\eta\frac{\partial u_1}{\partial x}\right) + \mu(u_1 - \bar{u}_1) + \phi^{u_1} + w^{u_1}\right)\right] + \frac{\partial^2 u_1}{\partial y^2} + \frac{1}{3}\frac{\partial}{\partial y}\left[\sigma(\mu(u_2 - \bar{u}_2) + \phi^{u_2})\right]\right],\end{aligned} \tag{4.2}$$

$$\begin{aligned}\frac{Du_2}{Dt} &+ (\gamma - 1)\left(\frac{T}{\rho}\frac{\partial \rho}{\partial y} + \frac{\partial T}{\partial y}\right) + u_2\sigma(\mu(u_2 - \bar{u}_2) + \phi^{u_2}) \\ &= \frac{1}{\mathrm{Re}\rho}\left[\eta^2\frac{\partial^2 u_2}{\partial x^2} + (\eta' + \sigma\mu)\eta\frac{\partial u_2}{\partial x} + \sigma\eta\frac{\partial \phi^{u_2}}{\partial x} + \sigma'\eta(\mu(u_2 - \bar{u}_2) + \phi^{u_2})\right. \\ &\left. + \sigma\left(\mu\left(\eta\frac{\partial u_2}{\partial x}\right) + \mu(u_2 - \bar{u}_2) + \phi^{u_2} + w^{u_2}\right) + \frac{4}{3}\frac{\partial^2 u_2}{\partial y^2} + \frac{1}{3}\frac{\partial}{\partial y}\left[\sigma(\mu(u_1 - \bar{u}_1) + \phi^{u_1})\right]\right],\end{aligned} \tag{4.3}$$

$$(4.4)\quad \frac{DT}{Dt} + u_1\sigma\left(\mu\left(T-\bar{T}\right)+\phi^T\right) + (\gamma-1)T\,\vec{\nabla}\cdot\vec{u} + (\gamma-1)T\sigma(\mu(u_1-\bar{u}_1)+\phi^{u_1})$$
$$= \frac{1}{\mathrm{Re}\,\rho}\left\{\frac{\gamma}{\mathrm{Pr}}\left[\eta^2\frac{\partial^2 T}{\partial x^2} + (\eta'+\sigma\mu)\eta\frac{\partial T}{\partial x} + \sigma\eta\frac{\partial \phi^T}{\partial x} + \sigma'\eta\left(\mu\left(T-\bar{T}\right)+\phi^T\right) + \frac{\partial^2 T}{\partial y^2}\right.\right.$$
$$\left.+\sigma\left(\mu\left(\eta\frac{\partial T}{\partial x}\right)+\mu\left(T-\bar{T}\right)+\phi^T+w^T\right)\right] + \frac{4}{3}\left[\left(\frac{\partial u_1}{\partial x}+\sigma(\mu(u_1-\bar{u}_1)+\phi^{u_1})\right)^2+\left(\frac{\partial u_2}{\partial y}\right)^2\right.$$
$$\left.\left.-\left(\frac{\partial u_1}{\partial x}+\sigma(\mu(u_1-\bar{u}_1)+\phi^{u_1})\right)\frac{\partial u_2}{\partial y}\right] + \left(\frac{\partial u_1}{\partial y}+\left(\frac{\partial u_2}{\partial x}+\sigma(\mu(u_2-\bar{u}_2)+\phi^{u_2})\right)\right)^2\right\},$$

$$(4.5)\quad \frac{\partial \phi^r}{\partial t} + \frac{\partial r}{\partial x} + u_2\frac{\partial r}{\partial y} + (\alpha+\sigma)(\mu(r-\bar{r})+\phi^r) = 0, \qquad r=\rho,u_1,u_2,T,$$

$$\frac{\partial w^r}{\partial t} + u_2\frac{\partial r}{\partial y} + (\eta'+\sigma\mu)\eta\frac{\partial r}{\partial x} + \sigma\eta\frac{\partial \phi^r}{\partial x} + \sigma'\eta(\mu(r-\bar{r})+\phi^r)$$
$$+\sigma\left(\mu\left(\eta\frac{\partial r}{\partial x}\right)+\mu(r-\bar{r})+\phi^r+w^r\right) = \eta^2\frac{\partial^2 r}{\partial x^2}, \qquad r=u_1,u_2,T.$$

**4.1. A numerical example: Convection of a vortex.** In this experiment we compute solutions to (3.9)–(3.12) on the domain $(x,y)\in[-10,10]\times[-10,10]$. We use $\mathrm{Re}=1000, \mathrm{Pr}=0.7$, $\gamma=1.4$, and consider a mean flow $\bar{\rho}=1$, $\bar{u}_1=0.3$ $\bar{T}=\frac{1}{\gamma}$. The initial data are the vortex

$$(4.6)\quad \rho = \bar{\rho}\left(1-\frac{(\gamma-1)A_v^2}{2}e^{1-x^2-y^2}\right)^{\frac{1}{\gamma-1}}, \qquad T=\bar{T}\left(1-\frac{(\gamma-1)A_v^2}{2}e^{1-x^2-y^2}\right),$$

$$(4.7)\quad u_1 = \bar{u}_1 - yA_v e^{\frac{1-x^2-y^2}{2}}, \qquad v_2 = xA_v e^{\frac{1-x^2-y^2}{2}}.$$

We choose $A_v=0.005$, which corresponds to a relatively weak vortex. It should be noted that, although the amplitude is relatively small, the solution to this problem (mainly a passive convection of the initial data along with the mean flow) is made possible only through nonlinear effects.

To test the nonlinear version of the PML we truncate the domain by adding a layer of width $L$ at $x=10$ (we terminate the layer with periodic boundary conditions so the setup is equivalent to adding two layers with half the width $L_{1/2}$ at $x=10$ and at $x=-10$). In the $y$-direction we use periodic boundary conditions.

We choose the damping functions $\sigma(x)$ and $\eta(x)$ as

$$\sigma(x) = \sigma_{\max}d(x), \qquad \eta(x) = \frac{1}{1+\eta_{\max}d(x)},$$

where

$$d(x) = e^{-\tau\left(\frac{x-x_c}{L_{1/2}}\right)^2} + e^{-\tau\left(\frac{x+x_c}{L_{1/2}}\right)^2},$$

with $x_c=12.5$ and $\tau=28$. As the damping functions now have global support, we solve (4.2)–(4.5) everywhere. (To maintain efficiency one could remove the auxiliary variables in regions where $d$ is negligibly small.) To assess the error we solve (3.9)–(3.12) on a larger domain $(x,y)\in[-50,50]\times[-10,10]$ in order to get a reference solution.

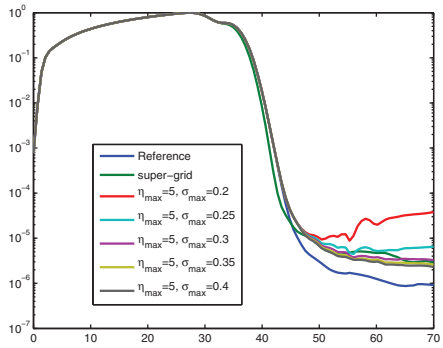


(a) The $L_2$ norm of the kinetic energy scaled by its maximum value. Here $\eta_{\max} = 5$ is fixed and $\sigma_{\max}$ is varied.

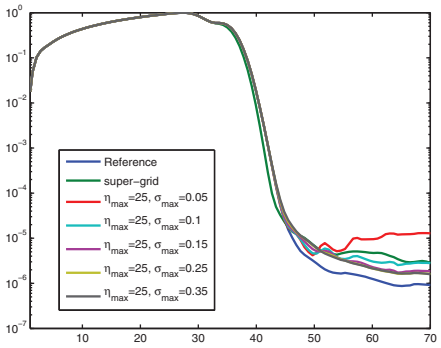


(b) The $L_2$ norm of the kinetic energy scaled by its maximum value. Here $\eta_{\max} = 25$ is fixed and $\sigma_{\max}$ is varied.

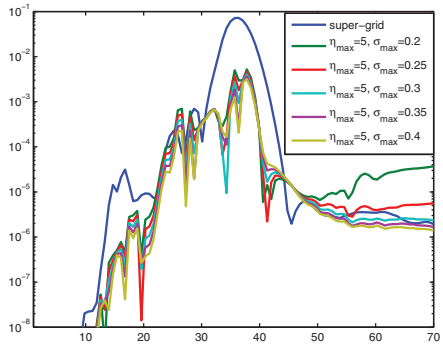


(c) The $L_2$ norm of the error in the kinetic energy scaled by the maximum value of the norm of the kinetic energy. Here $\eta_{\max} = 5$ is fixed and $\sigma_{\max}$ is varied.

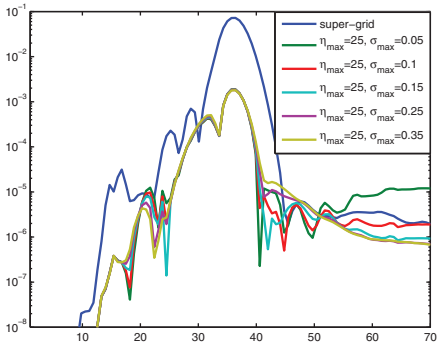


(d) The $L_2$ norm of the error in the kinetic energy scaled by the maximum value of the norm of the kinetic energy. Here $\eta_{\max} = 25$ is fixed and $\sigma_{\max}$ is varied.

FIG. 4.1. *All computations are done with* $L_{1/2} = 1.25$.

We discretize all equations using centered finite differences of order 12 with a grid spacing of 0.05 in both $x$ and $y$. To ensure stability of the reference problem (see [32]) we add a linear hyperviscosity term

$$\gamma h^{13} \left( \frac{\partial^{14} u}{\partial x^{14}} + \frac{\partial^{14} u}{\partial y^{14}} \right)$$

to the right-hand side of (4.1)–(4.4). In all computations we take $\gamma = -0.0012$. The time integration is performed by the classic fourth order accurate Runge–Kutta method, which is used to advance the solution to time 70 by taking 24000 time steps. The number of time steps was empirically determined so that the reference computation was stable. Thus, for this example, the layer does not introduce additional restrictions on the time step.

To evaluate our layer we try some different values of $\eta_{\max}$ and $\sigma_{\max}$ and monitor the $l_2$ norm of the kinetic energy of the perturbation and compare it to the reference solution. The results are found in Figure 4.1 where the kinetic energy, scaled by its maximum value, is plotted. In Figures 4.1(a) and (b) the results for fixed $\eta_{\max} = 5, 25$ and varying $\sigma_{\max}$ are displayed. In subfigures 4.1(c) and 4.1(d) the corresponding

TABLE 4.1

*Errors for various vortex strengths. The displayed error is the maximum error in the norm of the kinetic energy for different time intervals (e.g., $t = 0$ to $t = 10$) normalized by the maximum value (for all times) of the norm of the kinetic energy.*

| $A_v$ | 0-10 | 10-20 | 20-30 | 30-40 | 40-50 | 50-60 | 60-70 |
|---|---|---|---|---|---|---|---|
| 0.05 | 3.0(-9) | 2.4(-6) | 7.0(-4) | 7.6(-3) | 4.1(-4) | 5.6(-5) | 2.0(-5) |
| 0.10 | 3.6(-9) | 1.9(-6) | 2.3(-4) | 1.2(-2) | 7.1(-4) | 1.2(-4) | 4.7(-5) |
| 0.15 | 4.4(-9) | 2.7(-6) | 7.1(-5) | 1.2(-2) | 2.7(-3) | 1.8(-4) | 7.0(-5) |
| 0.20 | 5.4(-9) | 3.5(-6) | 5.3(-4) | 1.2(-2) | 5.3(-3) | 2.5(-4) | 1.0(-4) |
| 0.25 | 6.3(-9) | 3.9(-6) | 1.4(-3) | 1.0(-2) | 8.1(-3) | 2.5(-4) | 1.3(-4) |
| 0.30 | 7.3(-9) | 3.8(-6) | 2.3(-3) | 1.0(-2) | 9.9(-3) | 1.2(-4) | 1.0(-4) |
| 0.35 | 8.1(-9) | 3.7(-6) | 3.0(-3) | 1.1(-2) | 8.1(-3) | 6.5(-5) | 6.5(-5) |
| 0.40 | 8.9(-9) | 3.6(-6) | 3.1(-3) | 1.0(-2) | 3.0(-3) | 3.0(-4) | 6.4(-5) |
| 0.45 | 9.4(-9) | 3.5(-6) | 2.3(-3) | 5.8(-3) | 3.7(-3) | 4.2(-4) | 6.9(-5) |
| 0.50 | 9.6(-9) | 3.3(-6) | 1.6(-3) | 2.1(-3) | 1.5(-3) | 4.1(-4) | 2.3(-4) |

errors in the kinetic energy (again scaled by the maximum value of the kinetic energy) are plotted. The case with more stretching gives slightly better results; also it seems that the maximum error does not depend much on the damping parameter, but that errors at later times do.

We also compute solutions using Colonius' super grid scale boundary conditions [10] using the same number of points and the same damping functions in the super grid layer. The super grid layer gives a slightly larger error than the proposed layer, but on the other hand requires less memory and CPU.

**4.1.1. Effect of the strength of the vortex.** The setup of our final experiment is the same as the previous experiment with the following exceptions: the damping parameters are fixed to $\eta_{\max} = 15$ and $\sigma_{\max} = 0.3$, the Reynolds number is lower ($\mathrm{Re} = 200$), and the amplitude of the vortex is larger ($A_v = 0.05, 0.10, 0.15, \ldots, 0.50$). As in the previous experiment, we monitor the kinetic energy and compute the error compared to a reference solution computed on a larger domain. The results can be found in Table 4.1. The layer behaves consistently for all strengths of the vortex, and the error peaks at $\sim 1 \times 10^{-2}$ sometime between time 30 and 40, i.e., when the vortex starts to exit the domain. Contour plots displaying how the strongest vortex is absorbed by the layer can be found in Figure 4.2.

**4.2. Some remarks on stability.** For our nonlinear computations we don't have any theoretical stability results, but our experience (based on a relatively small number of tests) is that when the viscosity is large, the layer is robust and insensitive to the choices of the damping and stretching. For large Reynolds numbers and larger vortex strengths ($A_v > 0.35$) the layer model becomes more sensitive, and some choices of parameters made the computations blow up as the vortex entered the layer. However, for all Re tested, we could always find a set of parameters that gave a stable solution with a reasonable result. As a final remark, we note that for the corresponding nonviscous problem we have not had any problems with instabilities [17].

**4.3. Some remarks on the limitations and extensions of the PML models for the linearized Navier–Stokes and Navier–Stokes equations.** As was pointed out by one of the anonymous referees, the above models are somewhat limited, as they consider only the case of single PML for a uniform mean flow aligned with the $x_1$-axis. Some of the challenges in extending the present model are

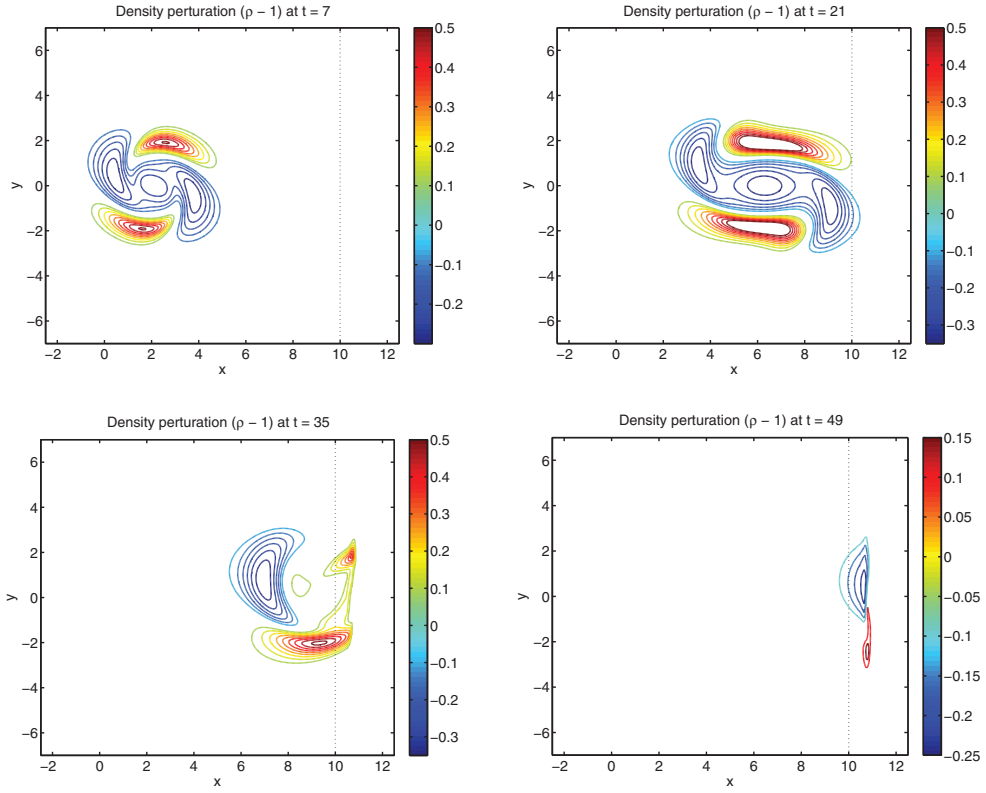


FIG. 4.2. *Contour plots at various times of the density perturbation* $\rho - 1$ *for the strongest vortex* $A_v = 0.5$. *The dotted line marks the start of the layer.*

1. the ability to construct stable PMLs in corners for oblique flow;
2. how to choose the parameter $\mu$ for nonconstant and nonlinear flows.

Presently, we do not have answers to these questions, but we note that for the hyperbolic case, these problems have been studied in the literature; see, for example, [27, 23, 26, 28]. We hope that the techniques there can be carried over to the hyperbolic-parabolic case, although we have not performed such analysis yet.

**5. Summary.** We have presented a very general PML model for hyperbolic-parabolic systems and applied it to both linear and nonlinear problems. For linear problems we have proved that the new hyperbolic-parabolic layer is perfectly matched to the governing equations. We have seen that if a standard hyperbolic PML is used for a mixed hyperbolic-parabolic problem, the perfect matching is lost. This causes a significant degradation in performance. In fact, the numerical examples with our linear applications show that our new layer can be up to six orders of magnitude better. We have also shown how the new layer can be used for nonlinear problems by applying it to the compressible Navier–Stokes equations. For nonlinear applications the perfect matching is lost, and the performance of the layer cannot be expected to be as good as for a linear application. Nevertheless, in our numerical experiments we see that the new layer behaves consistently and is competitive with respect to a more standard damping layer.

## Appendix.

### A.1. A PML in two directions for the damped wave equation.

$$\frac{\partial v}{\partial t} = \frac{\partial w}{\partial x} + \sigma_x \phi_x^{(w)} + \frac{\partial p}{\partial y} + \sigma_y \phi_y^{(p)} + \varepsilon \left( \frac{\partial^2 v}{\partial x^2} + \frac{\partial^2 v}{\partial y^2} + \frac{\partial \left( \sigma_x \phi_x^{(v)} \right)}{\partial x} + \sigma_x \varphi_x^{(v)} + \frac{\partial \left( \sigma_y \phi_y^{(v)} \right)}{\partial y} + \sigma_y \varphi_y^{(v)} \right), \tag{A.1}$$

$$\frac{\partial w}{\partial t} = \frac{\partial v}{\partial x} + \sigma_x \phi_x^{(v)}, \tag{A.2}$$

$$\frac{\partial p}{\partial t} = \frac{\partial v}{\partial y} + \sigma_y \phi_y^{(v)}, \tag{A.3}$$

$$\frac{\partial \phi_x^{(v)}}{\partial t} + (\sigma_x + \beta)\phi_x^{(v)} = -\frac{\partial v}{\partial x}, \tag{A.4}$$

$$\frac{\partial \phi_x^{(w)}}{\partial t} + (\sigma_x + \beta)\phi_x^{(w)} = -\frac{\partial w}{\partial x}, \tag{A.5}$$

$$\frac{\partial \varphi_x^{(v)}}{\partial t} + (\sigma_x + \beta)\varphi_x^{(v)} = -\left( \frac{\partial^2 v}{\partial x^2} + \frac{\partial (\sigma_x \phi_x^{(v)})}{\partial x} \right), \tag{A.6}$$

$$\frac{\partial \phi_y^{(v)}}{\partial t} + (\sigma_y + \beta)\phi_y^{(v)} = -\frac{\partial v}{\partial y}, \tag{A.7}$$

$$\frac{\partial \phi_y^{(p)}}{\partial t} + (\sigma_y + \beta)\phi_y^{(p)} = -\frac{\partial p}{\partial y}, \tag{A.8}$$

$$\frac{\partial \varphi_y^{(v)}}{\partial t} + (\sigma_y + \beta)\varphi_y^{(v)} = -\left( \frac{\partial^2 v}{\partial y^2} + \frac{\partial \left( \sigma_y \phi_y^{(v)} \right)}{\partial y} \right). \tag{A.9}$$

## REFERENCES


[1] S. Abarbanel and D. Gottlieb, *A mathematical analysis of the PML method*, J. Comput. Phys., 134 (1997), pp. 357–363.

[2] S. Abarbanel and D. Gottlieb, *On the construction and analysis of absorbing layers in CEM*, Appl. Numer. Math., 27 (1998), pp. 331–340.

[3] S. Abarbanel, D. Gottlieb, and J. Hesthaven, *Long time behaviour of the perfectly matched layer equations in computational electromagnetics*, J. Sci. Comput., 17 (2002), pp. 405–422.

[4] D. Appelö and T. Hagstrom, *Construction of stable PMLs for general* $2 \times 2$ *symmetric hyperbolic systems*, in Proceedings of the Tenth International Conference on Hyperbolic Problems: Theory, Numerics, Applications, Osaka, 2004, submitted.

[5] D. Appelö, T. Hagstrom, and G. Kreiss, *Perfectly matched layers for hyperbolic systems: General formulation, well-posedness, and stability*, SIAM J. Appl. Math., 67 (2006), pp. 1–23.

[6] E. Bécache, S. Fauqueux, and P. Joly, *Stability of perfectly matched layers, group velocities and anisotropic waves*, J. Comput. Phys., 188 (2003), pp. 399–433.

[7] J. Bérenger, *A perfectly matched layer for the absorption of electromagnetic waves*, J. Comput. Phys., 114 (1994), pp. 185–200.

[8] D. J. Bodony, *Analysis of sponge zones for computational fluid mechanics*, J. Comput. Phys., 212 (2006), pp. 681–702.

[9] F. Collino, *Perfectly matched absorbing layers for the paraxial equations*, J. Comput. Phys., 113 (1997), pp. 164–180.

[10] T. Colonius and H. Ran, *A super-grid-scale model for simulating compressible flow on unbounded domains*, J. Comput. Phys., 182 (2002), pp. 191–212.

[11] B. Engquist and A. Majda, *Absorbing boundary conditions for the numerical simulation of waves*, Math. Comp., 31 (1977), pp. 629–651.

[12] T. Hagstrom, *Asymptotic boundary conditions for dissipative waves: General theory*, Math. Comp., 56 (1991), pp. 589–606.
[13] T. Hagstrom, *Radiation boundary conditions for the numerical simulation of waves*, Acta Numer., 8 (1999), pp. 47–106.
[14] T. Hagstrom, *New results on absorbing layers and radiation boundary conditions*, in Lect. Notes Comput. Sci. Eng. 31, M. Ainsworth, P. Davies, D. Duncan, P. Martin, and B. Rynne, eds., Springer-Verlag, New York, 2003; Topics in Computational Wave Propagation, Springer-Verlag, New York, 2003, pp. 1–42.
[15] T. Hagstrom, *Summary of Solutions to Category* 1 *Benchmark Problem on Boundary Treatments for the Linearized Euler Equations*, in Proceedings of the 4th CAA Workshop on Benchmark Problems, 2003.
[16] T. Hagstrom and D. Appelö, *Automatic symmetrization and energy estimates using local operators for partial differential equations*, Comm. Partial Differential Equations, 32 (2007), pp. 1129–1145.
[17] T. Hagstrom and D. Appelö, *Experiments with Hermite methods for simulating compressible flows: Runge-Kutta time-stepping and absorbing layers*, in Proceedings of the 13th AIAA/CEAS Aeroacoustics Conference, 2007.
[18] T. Hagstrom, J. Goodrich, I. Nazarov, and C. Dodson, *High-order methods and boundary conditions for simulating subsonic flows*, in Proceedings of the 11th AIAA/CEAS Aeroacoustics Conference, 2005.
[19] T. Hagstrom, J. Goodrich, and G. Zhu, *A Hermite-Taylor algorithm for simulating subsonic shear flows*, in Proceedings of the 12th AIAA/CEAS Aeroacoustics Conference, 2006.
[20] T. Hagstrom and S. Lau, *Radiation boundary conditions for Maxwell's equations: A review of accurate time-domain formulations*, J. Comput. Math., 25 (2007), pp. 305–336.
[21] L. Halpern, *Artificial boundary conditions for incompletely parabolic perturbations of hyperbolic systems*, SIAM J. Math. Anal., 22 (1991), pp. 1256–1283.
[22] F. Q. Hu, *On absorbing boundary conditions for linearized Euler equations by a perfectly matched layer*, J. Comput. Phys., 129 (1996), pp. 201–209.
[23] F. Q. Hu, *A perfectly matched layer absorbing boundary condition for linearized Euler equations with a non-uniform mean flow*, J. Comput. Phys., 208 (2005), pp. 469–492.
[24] F. Q. Hu, *On the Construction of PML Absorbing Boundary Condition for the Non-linear Euler Equations*, Technical report 2006-0798, 44th AIAA Aerospace Sciences Meeting and Exhibit, Reno, NV, 2006.
[25] M. Israeli and S. Orzag, *Approximation of radiation boundary conditions*, J. Comput. Phys., 41 (1981), pp. 115–135.
[26] F. Nataf, *A new approach to perfectly matched layers for the linearized Euler system*, J. Comput. Phys., 214 (2006), pp. 757–772.
[27] I. Nazarov, I. *A Mathematical Analysis for Sustainable Ecosystems,* II. *Perfectly Matched Layers for Linearized Euler's Equations*, Ph.D. thesis, University of New Mexico, Albuquerque, NM, 2004.
[28] S. Parrish and F. Q. Hu, *Application of PML absorbing boundary condition to aeroacoustics problems with an oblique mean flow*, in Proceedings of the 13th AIAA/CEAS Aeroacoustics Conference, 2007.
[29] C. Tsitouras and S. N. Papakostas, *Cheap error estimation for Runge–Kutta methods*, SIAM J. Sci. Comput., 20 (1999), pp. 2067–2088.
[30] S. Tsynkov, *Numerical solution of problems on unbounded domains, a review*, Appl. Numer. Math., 27 (1998), pp. 465–532.
[31] C. W.C. and L. Q. H., *Perfectly matched layers for elastodynamics: A new absorbing boundary condition*, J. Comput. Acoust., 4 (1996), pp. 341–359.
[32] H. Yee, M. Vinokur, and M. Djomehri, *Entropy splitting and numerical dissipation*, J. Comput. Phys., 162 (2000), pp. 33–81.